

Iterative Event-based Motion Segmentation by Variational Contrast Maximization

Ryo Yamaki¹, Shintaro Shiba^{1,2}, Guillermo Gallego^{2,3}, and Yoshimitsu Aoki¹
¹ Keio University, Japan, ² Technische Universität Berlin, ³ Einstein Center Digital Future,
Robotics Institute Germany, and Science of Intelligence Excellence Cluster, Germany.

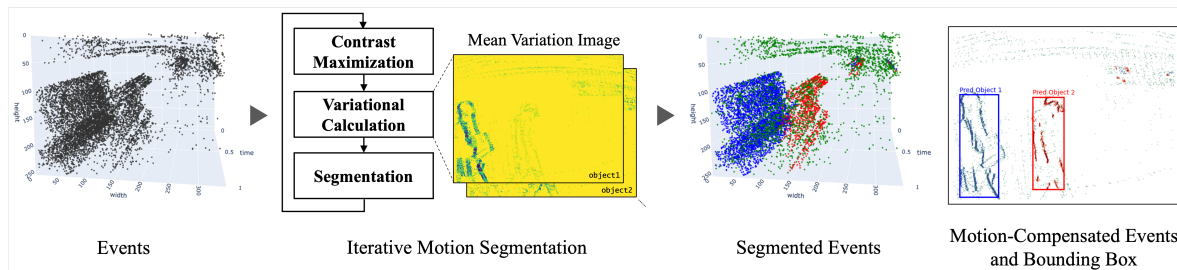


Figure 1. *Overview.* The proposed method relies on event data, and achieves motion segmentation by iteratively running Contrast Maximization with respect to the parameters *and* with respect to the event data. The variation can be visualized as Mean Variation Image. As results, we obtain the segmented event stream and motion-compensated images (i.e., images of warped events). The scene (from [47]) shows two pedestrians walking in a corridor while the camera slightly moves.

Abstract

Event cameras provide rich signals that are suitable for motion estimation since they respond to changes in the scene. As any visual changes in the scene produce event data, it is paramount to classify the data into different motions (i.e., motion segmentation), which is useful for various tasks such as object detection and visual servoing. We propose an iterative motion segmentation method, by classifying events into background (e.g., dominant motion hypothesis) and foreground (independent motion residuals), thus extending the Contrast Maximization framework. Experimental results demonstrate that the proposed method successfully classifies event clusters both for public and self-recorded datasets, producing sharp, motion-compensated edge-like images. The proposed method achieves state-of-the-art accuracy on moving object detection benchmarks with an improvement of over 30%, and demonstrates its possibility of applying to more complex and noisy real-world scenes. We hope this work broadens the sensitivity of Contrast Maximization with respect to both motion parameters and input events, thus contributing to theoretical advancements in event-based motion segmentation estimation. https://github.com/aoki-media-lab/event_based_segmentation_vcmax

1. Introduction

Event cameras are bio-inspired vision sensors that provide asynchronous responses to the motion of edges with high dynamic range (HDR) and minimal blur at high temporal (μs) resolution [33]. The signals from event cameras are naturally suitable for motion estimation, especially in challenging real-world scenarios for conventional (frame-based) cameras. Segmenting different scene motions in image space is a paramount task for various downstream tasks, such as object detection and visual servoing.

Motion segmentation for event cameras classifies each event into different clusters that represent the motions of the objects causing the events. However, since event cameras produce a high-dimensional output stream (“events”) due to their asynchronous working principle, finding different motion clusters in the event stream is a challenging task. Conventional frame-based methods cannot be easily adapted to event data as the data types are fundamentally different [10]. In some previous event-based motion segmentation methods, the number of clusters is predetermined. For example, [40] proposed a method based on the Contrast Maximization (CMax) framework [8] to simultaneously optimize two sets of unknowns: the motion parameters of each cluster and the probability that each event belongs to each cluster. However, providing the number of clusters for a new scene

	Mitrokhin et al. [20]	EMSMC [40]	EMSGC [47]	This work
Problem unknowns	Motion parameters $\{\theta_j\}_{j=1}^{N_c}$, per-pixel cluster labels $\{\ell_x\}$, $\ell_x \in \{1, \dots, N_c\}$	Motion parameters $\{\theta_j\}_{j=1}^{N_c}$, per-event cluster probabilities $\{p_{kj}\}$	Motion parameters $\{\theta_j\}_{j=1}^{N_c}$, per-event cluster labels $\{\ell_k\}$, $\ell_k \in \{1, \dots, N_c\}$	Motion clusters $\{\theta_j, \mathcal{E}_j\}_{j=1}^{N_c}$ (same meaning as EMSGC)
Number of clusters N_c	Automatically computed (by detection hyper-parameters).	Given	Automatically computed (by means of MDL loss term)	Automatically computed
Objective function	Event alignment (\approx CMax)	Motion compensation (CMax)	Motion compensation (CMax) and two priors (Potts & MDL)	Motion compensation (CMax)
Estimation approach	Greedy (dominant motion and residuals)	Joint, by Expectation-Maximization	Joint, by alternating solvers on a Markov Random Field	Greedy (dominant motion and residuals)
Optimization method	Gradient descent and thresholding	Conjugate gradient and “closed-form” formula	Conjugate gradient and graph cut	Conjugate gradient and thresholding
Motion estimation	Motion compensation on residual events	CMax with probabilities p_{kj} (using weighted IWEs)	CMax using selected events per cluster	CMax on residual events
Event-cluster associations	Hard (0 or 1, dominant motion or residuals)	Soft (probabilities p_{kj})	Hard $\ell_k \in \{1, \dots, N_c\}$	Hard (0 or 1, dominant motion or residuals)
Segmentation (Classification)	Per-pixel, by thresholding time-surface dispersion.	Per-event, closed-form partition-of-unity formula based on local contrast	Per-event, using a graph through the events and graph cut(s)	Per-event, by thresholding the loss variation

Table 1. Comparison of event-based motion segmentation methods based on the CMax framework.

is not straightforward. Hence, it is paramount to develop methods that iteratively segment motion clusters by classifying events into different clusters.

In this work, we propose a novel algorithm that classifies events iteratively to achieve motion segmentation, extending the CMax framework (Fig. 1). The proposed variational approach defines the scores about how much each event aligns with the current motion hypothesis after estimating the dominant motion of the scene, and it runs iteratively on the events that do not conform to the dominant motion (i.e., rest of events or “residual events”). Experimental results demonstrate that the proposed method successfully classifies event clusters both for simple datasets and public datasets, producing sharp, motion-compensated images. Also, the proposed method is useful for object detection, where it achieves the state-of-the-art bounding box accuracy by 30% improvement.

Our contributions can be summarized as follows:

1. We propose a novel method to classify events with a given motion hypothesis, based on the strength of the first variation of the CMax loss function with respect to the events (Sec. 3.3).
2. We propose an iterative motion segmentation with the above classification, by estimating dominant motion of the current events and the residual events that do not support the dominant motion (Sec. 3).
3. We conduct comprehensive experiments on four different datasets, evaluating on simple scenes and real-world data, showcasing the efficacy of the proposed method on both motion segmentation and object detection (Sec. 4).

2. Related Work

Event-based motion segmentation is a task that classifies events into different motion clusters. Prior work can be categorized into model-based and learning-based approaches. Model-based approaches cluster the input events (spatio-temporal stream) that best aligns with different motions. Extending the CMax framework [7–9], Stoffregen et al. [40] propose “Event-based Motion Segmentation by Motion Compensation” (EMSMC), an Expectation-Maximization (EM) algorithm that estimates the motion parameters and the event-cluster classification probabilities at the same time, maximizing the contrast of a compound image of warped events (IWE). In [29], motion compensation is combined with feature tracking, repeatedly fitting and merging models with a scene segmented into multiple motions. Zhou et al. [47] propose an optimization method using a graph-cut technique for clustering events. They also propose a new dataset for the task.

Learning-based methods predict independently-moving object (IMO) masks, or alternatively predict other quantities (e.g., optical flow, scene depth, etc.) and estimate IMOs from them [1–3, 44, 46]. A typical approach uses optical flow networks before clustering IMOs, such as unsupervised-learning-based method [44]. Other scene quantities, such as semantic labels [16] and the scene depth and camera pose [11], can also be utilized. Works like [5, 21] follow this approach and release the de-facto standard dataset (EVIMO). Recently, the spatio-temporal characteristics of event data are further investigated, by exploring model architectures, such as graph convolutional net-

work [22] and spiking neural networks [28]. Additionally, Zhou et al. [46] propose a spatio-temporal joint inference method, focusing on the cylindrical shape formed by IMO in the space-time domain of the image plane.

Our optimization-based method is most related to EMSMC [40], where the expectation-maximization method is combined with the CMax framework. However, we propose an iterative approach that mitigates the dependency on the number of clusters and the initial values for the optimization, resulting in state-of-the-art accuracy in both motion segmentation and object detection. Table 1 summarizes the characteristics of the closely related but different approaches. A more technical comparison is presented at the end of Sec. 3.3, after explaining our approach.

3. Method

In this section, first, we revisit the principles of event cameras (Sec. 3.1). Then, we cover the CMax framework (Sec. 3.2), which is the basis of the proposed method. The variational approach and motion segmentation method are explained in Sec. 3.3.

3.1. Event Cameras

Instead of acquiring brightness images at fixed time intervals (e.g., frames), event cameras record brightness changes asynchronously, called “events” [10, 19]. An event $e_k \doteq (\mathbf{x}_k, t_k, p_k)$ is triggered as soon as the logarithmic brightness at the pixel $\mathbf{x}_k \doteq (x_k, y_k)^\top$ exceeds a preset threshold (i.e., contrast sensitivity) C . Here, t_k is the timestamp of the event with μs resolution, and polarity $p_k \in \{+1, -1\}$ is the sign of the brightness change:

$$L(\mathbf{x}_k, t_k) - L(\mathbf{x}_k, t_k - \Delta t_k) = p_k C. \quad (1)$$

3.2. Contrast Maximization

The CMax framework [7–9] is powerful for various motion-estimation tasks, such as rotational motion [7, 12, 13, 17, 35], homographic motion [8, 26, 32], optical flow [14, 15, 30, 31, 36, 38], and motion segmentation [20, 29, 40, 47]. The first step in CMax is to transform input events $\mathcal{E} = \{e_k\}_{k=1}^{N_e}$ to warped events $\mathcal{E}' = \{e'_k\}_{k=1}^{N_e}$ using a motion model \mathbf{W} ,

$$e_k \doteq (\mathbf{x}_k, t_k, p_k) \xrightarrow{\mathbf{W}} e'_k \doteq (\mathbf{x}'_k, t_{\text{ref}}, p_k). \quad (2)$$

The warp $\mathbf{x}'_k = \mathbf{W}(\mathbf{x}_k, t_k; \theta)$ transports each event along the point trajectory that passes through it, until the reference time t_{ref} is reached. The point trajectories are parametrized by θ , which is based on the motion model for estimation. Then, an objective function (e.g., image contrast) [9, 39] measures the alignment of the warped events \mathcal{E}' . Many objective functions are defined in terms of the histogram of the

warped events, or the image of warped events (IWE):

$$\text{IWE}(\mathbf{x}; \theta) \doteq \sum_{k=1}^{N_e} b_k \delta(\mathbf{x} - \mathbf{x}'_k(\theta)). \quad (3)$$

Each IWE pixel \mathbf{x} sums the values of the warped events \mathbf{x}'_k that fall within it. $b_k = p_k$ if polarity is used or $b_k = 1$ if polarity is not used. The Dirac delta δ is in practice replaced by a smooth approximation [25], such as a Gaussian, $\delta(\mathbf{x} - \mu) \approx \mathcal{N}(\mathbf{x}; \mu, \epsilon^2)$ with $\epsilon = 1$ pixel. A popular objective function $\mathcal{L}(\theta)$ is the variance of the IWE (3):

$$\mathcal{L}(\theta) \equiv \frac{1}{|\Omega|} \int_{\Omega} (\text{IWE}(\mathbf{x}; \theta) - \mu)^2 d\mathbf{x}, \quad (4)$$

with mean $\mu \doteq \frac{1}{|\Omega|} \int_{\Omega} \text{IWE}(\mathbf{x}; \theta) d\mathbf{x}$ over the image domain Ω . Hence, the alignment of the transformed events \mathcal{E}' (i.e., the candidate “corresponding events”, triggered by the same scene edge) is measured by the strength of the edges of the IWE.

Finally, an optimization algorithm iterates the above steps until the best parameters are found:

$$\theta^* = \arg \max_{\theta} \mathcal{L}(\theta). \quad (5)$$

As an intuitive interpretation, when the candidate motion is correct, each warped event overlaps at the reference time t_{ref} , resulting in an image that clearly presents the edges at the moment of t_{ref} . On the other hand, if the candidate motion does not match the actual motion of the object, a low-contrast, blurred IWE is produced.

3.3. Segmentation using the Calculus of Variations

Accounting for multiple motions in the scene. In CMax, the warp \mathbf{W} defines the type of motion (motion hypothesis, which is a design choice), that is parametrized by θ . For instance, when the entire image plane is assumed to move with a common linear velocity, the warp is a two-dimensional translation $\mathbf{x}'_k = \mathbf{x}_k - (t_k - t_{\text{ref}})\mathbf{v}$ and $\theta \doteq \mathbf{v} = (v_x, v_y)^\top$ is the velocity. However, when two or more IMOs are present in the scene, a motion hypothesis like the one above, with two degrees of freedom (DOFs), cannot fully explain the event data. In practice, it is not easy to design a warp that covers a wide range of scenes; this requires warps with many DOFs (e.g., optical flow). And it is also not easy to estimate its best parameters θ^* : high-DOF problems are more ill-conditioned than low-DOF ones. Hence, instead of estimating all motions (DOFs) at once, we proceed to segment different motions iteratively, by determining which parts of the event data fit the simple motion model $\theta \doteq \mathbf{v}$, and fitting new motion parameters to the residual events that do not align with the previous estimation.

Proposed Approach. Our method is summarized in Fig. 2 and Algorithm 1. Instead of seeking the optimal

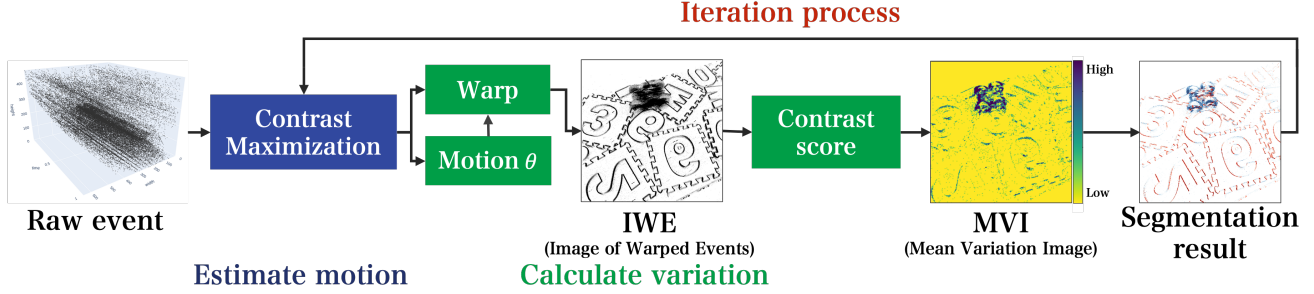


Figure 2. *Block diagram of the proposed method.* First, we use Contrast Maximization to estimate the dominant motion on the scene. Using the estimated motion θ , we calculate the first variation of the contrast function with respect to the event coordinates (6). The magnitude of the first variation can be visualized as a heat map (7) (here, from yellow to blue): the higher it is, the greater the likelihood that the corresponding events do not conform to the estimated motion, i.e., they belong to an independent moving object (IMO). Thresholding the first variation classifies events into the “fit” events and “residual” events in terms of the currently estimated motion. The “fit” events are removed (defining a segmented object or “cluster”) and the above steps are repeated on the residual events, until the final segmentation.

Algorithm 1 Iterative Motion Segmentation Algorithm

Input: Events \mathcal{E} , threshold T

Output: Motion clusters and best motion parameters

$\{\mathcal{E}_i, \theta_i^*\}_{i=1}^{N_{\text{cluster}}}$

- 1: Initialize residual events $\mathcal{E}^{\text{res}} = \mathcal{E}$, $N_{\text{cluster}} = 0$, $i = 1$.
 - 2: **while** $\mathcal{E}^{\text{res}} \neq \emptyset$ **do**
 - 3: Estimate motion θ^* using Contrast Maximization (5) or external sensors (e.g., IMU)
 - 4: Warp events (2) \mathcal{E}^{res}
 - 5: Calculate the gradient (6)
 - 6: Obtain the current cluster (segment): $\theta_i^* = \theta^*$ and $\mathcal{E}_i = \{e_k\}$ s.t. $\|\frac{\partial \mathcal{L}(\mathbf{x}_k; \theta_i^*)}{\partial \mathbf{x}_k}\| > T$
 - 7: $N_{\text{cluster}} \leftarrow N_{\text{cluster}} + 1$
 - 8: Update events using the residuals $\mathcal{E}^{\text{res}} \leftarrow \{e_k\}$ s.t. $\|\frac{\partial \mathcal{L}(\mathbf{x}_k; \theta^*)}{\partial \mathbf{x}_k}\| < T$.
 - 9: $i \leftarrow i + 1$
 - 10: **end while**
-

motion θ^* , we assume that the motion parameters θ are already known with certain accuracy. The parameters θ can be given either by a step of CMax (see Sec. 4.3 for the results) or by other sensors (e.g., LiDAR or IMU) (see Sec. 4.4 for the results). In either case, we assume θ represents the dominant motion for the current event data (e.g., ego-motion-induced events, excluding IMOs). To define the “goodness of fit” of events with respect to the current motion θ , we are inspired by the Calculus of Variations [6], proposing a variational method to classify events based on the motion parameters. In CMax (5), θ^* may be found iteratively by following the gradient $\partial \mathcal{L} / \partial \theta$, e.g., as in steepest ascent $\theta \leftarrow \theta + \mu \frac{\partial \mathcal{L}}{\partial \theta}$ (with $\mu \geq 0$).

Complementary, the variational approach looks at the sensitivity of the objective function with respect to the

events, assuming fixed motion parameters θ :

$$\frac{\partial \mathcal{L}(\mathbf{x}_k; \theta)}{\partial \mathbf{x}_k} = \left(\frac{\partial \mathcal{L}(\mathbf{x}_k; \theta)}{\partial x_k}, \frac{\partial \mathcal{L}(\mathbf{x}_k; \theta)}{\partial y_k} \right). \quad (6)$$

Intuitively, it evaluates how the coordinates of each event affect the contrast function assuming θ is fixed, and it can be leveraged to increase the contrast score. If an event is aligned with the point trajectories of the current motion θ , then the variation (6) should be large, while if it is not aligned (e.g., IMOs), the variation should be close to zero.

In practice, to calculate the per-event variation (6) we rely on automatic differentiation libraries, such as PyTorch. The magnitude of the variation, $\|\partial \mathcal{L}(\mathbf{x}_k; \theta) / \partial \mathbf{x}_k\|$, informs about how much the event matches the motion hypothesis θ . By thresholding it at some level T , we thus classify the events into those agreeing with the current motion and the residuals (Algorithm 1, line 6). This process of determining the dominant motion and classifying events is subsequently repeated for the residual events (segmentation iteration), until the number of residual events becomes negligibly small (i.e., noise). The threshold T can be predetermined, or decided statistically using Otsu’s algorithm [27] on the histogram of values $\{\|\partial \mathcal{L} / \partial \mathbf{x}_k\|\}$. We analyse the histogram and discuss more details in the supplementary.

Visualization. To visualize (6), we may build an image (e.g., akin to the IWE) by taking per-pixel averages, e.g., such as the “mean (magnitude) variation image” (MVI):

$$\text{MVI}(\mathcal{E}, \theta) \doteq \frac{1}{N_e(\mathbf{x})} \sum_{k=1}^{N_e} \left\| \frac{\partial \mathcal{L}(\mathbf{x}_k; \theta)}{\partial \mathbf{x}_k} \right\| \delta(\mathbf{x} - \mathbf{x}'_k), \quad (7)$$

where $N_e(\mathbf{x}) \doteq \sum_{k=1}^{N_e} \delta(\mathbf{x} - \mathbf{x}'_k)$ is the number of warped events at pixel \mathbf{x} (the IWE). An example of the MVI is shown in Fig. 2, colored from yellow (low) to blue (high).

Technical comparison with prior work. Similarly to prior work, our method is based on CMax, without requiring external labels (Tab. 1). However, there are some differences. EMSMC [40] uses event probabilities p_{kj} as weights during IWE calculation, whereas our approach does not; our resulting event probabilities are 0 or 1 (the events belong to one cluster or to another). Another difference with respect to EMSMC is the character of the iterative process. Our approach revitalizes the idea of the “greedy” strategy of [20], obtaining the clusters sequentially, in decreasing order of dominance, as measured by the number of events that conform with the newly estimated motion. This is faster than EMSMC, which follows an EM (i.e., non-greedy) approach: all motion clusters may change in every EM iteration. Differently from EMSGC [47] (also in Tab. 1), we do not need to build a graph of events and find the best partition of the graph to classify events into the IMOs. The number of clusters is automatically determined via the iteration, instead of by energy minimization.

4. Experiment

In this section, first we describe the datasets (Sec. 4.1) and the assessment metrics as well as hyper-parameters (Sec. 4.2). Then, we report on two different evaluations: motion segmentation using self-recorded simple datasets (Sec. 4.3) and moving-object detection (Secs. 4.4 and 4.5), both using real-world datasets.

4.1. Datasets

Self-recorded Dataset. To show the efficacy of the proposed method, we first use self-recorded data that consist of simple scenes with different IMO patterns. The dataset, acquired with a DAVIS346 [42], comprises events and images of 346×260 pixels. The camera is static and looks downward and front-to-parallel to the ground, capturing multiple objects (such as cylinders and toy trains) moving with approximately constant linear velocities. We record seven sequences that vary the types of objects, their motion directions (e.g., parallel, opposite, vertical) and speeds. The dataset contains over 2 million events in total.

EVIMO2 [5] consists of 41 minutes of data from three event cameras (640×480 pixels), one RGB camera, two IMUs, and accurate object poses from a motion capture system. We use three sequences (*scene13_dyn_test_00*, *scene10_dyn_train_00* and *scene15_dyn_test_02*) to evaluate IMOs following previous works [46]. Depth and segmentation of the scene, including objects, are provided from the event camera viewpoint at 60 Hz, which we use to warp the initial motion cluster. For each sequence we select time slices that include one IMO, hence we evaluate 1.3M events over 0.76 seconds.

EMSGC [47] consists of small camera motions and several IMOs in the scene, which are recorded using a hand-

held DAVIS346 camera. We test some real-world sequences following previous work [47].

ECD [23] is a standard dataset for various camera ego-motion estimation [7, 24, 34, 48]. Using a DAVIS240C camera (240×180 px [4]), each sequence provides events, frames, calibration information, IMU data, and ground truth (GT) camera poses (at 200 Hz). We use *dynamic_rotation* that includes IMOs (a person moving objects).

4.2. Evaluation Metrics and Hyper-parameters

FWL. We use the Flow Warp Loss (FWL) [41] for evaluating motion segmentation results. The FWL is defined as the ratio of the variance of IWE with respect to the variance of the original event image (i.e., IWE of no warp):

$$\text{FWL} \doteq \frac{\sigma^2(\text{IWE}(\mathbf{x}; \boldsymbol{\theta}))}{\sigma^2(\text{IWE}(\mathbf{x}; \mathbf{0}))}. \quad (8)$$

It is interpreted as follows: an $\text{FWL} > 1$ indicates that the output IWE has higher contrast than the input IWE, implying that the events are better aligned and segmented to different motions. Without the event collapse phenomenon [35], which is avoided because the warps used are well-behaved [37], higher FWL is better.

Intersection over Union (IoU) is a widely used metric for evaluating the accuracy of object detection and segmentation. It measures the overlap between the predicted segmentation P (motion cluster or its bounding box) and the ground truth G . Specifically, IoU is defined as the ratio of the intersection area of the predicted and ground truth (GT) regions to their union area:

$$\text{IoU} \doteq \frac{|P \cap G|}{|P \cup G|}. \quad (9)$$

$\text{IoU} = 1$ indicates perfect overlap between the prediction and GT, while $\text{IoU} = 0$ indicates no overlap. High IoU values indicate better segmentation or detection accuracy.

Hyper-parameters. We use various motion models for the camera ego-motion to test the efficacy of the proposed method: 2-DOF feature flow for the self-recorded and EMSGC datasets where the camera is static (almost static for EMSGC), use the static-scene depth and ego-motion parameterization (i.e., motion field that has $N_p + 6$ DOFs, where N_p is the number of pixels) for the EVIMO2 dataset (see Sec. 4.4), and use the 3-DOF rotational motion for the ECD dataset. Also, in one event slice, we use events 10 ms for the self-recorded dataset, 50 ms for the EVIMO2 experiments, and Adam [18] with the learning rate of 0.5 as the optimizer. We leave the further parameter details to the released implementation.

4.3. Motion Segmentation

Figure 3 shows the results of the iterative motion segmentation on the self-recorded dataset. The mean variation images (MVIs) clearly show that the first variation becomes

	cylinder1		cylinder2		toy1		toy2		toy3		toy4		toy5	
	FWL	IoU												
EMSMC [40] <i>zero init.</i>	1.01	0.34	1.32	<u>0.56</u>	<u>1.12</u>	0.18	0.94	0.62	0.94	0.28	1.31	0.62	<u>1.37</u>	0.26
EMSMC [40] <i>random init.</i>	1.24	<u>0.50</u>	1.20	0.55	1.00	0.23	1.96	<u>0.74</u>	<u>1.10</u>	0.67	1.26	<u>0.63</u>	1.33	<u>0.27</u>
EMSGC [47]	1.09	–	<u>1.33</u>	–	1.08	–	1.68	–	1.06	–	<u>1.34</u>	–	1.18	–
Ours (<i>zero init.</i>)	<u>1.16</u>	0.63	1.40	0.81	1.14	<u>0.19</u>	<u>1.79</u>	0.83	1.13	<u>0.61</u>	1.56	0.73	1.40	0.31

Table 2. *Quantitative results on self-recorded dataset.* Higher FWL and IoU values indicate better segmentation. The EM-based algorithm (EMSMC) [40] relies on the initial value of the motion, while ours achieves high FWL and IoU values without initialization (i.e., zero).

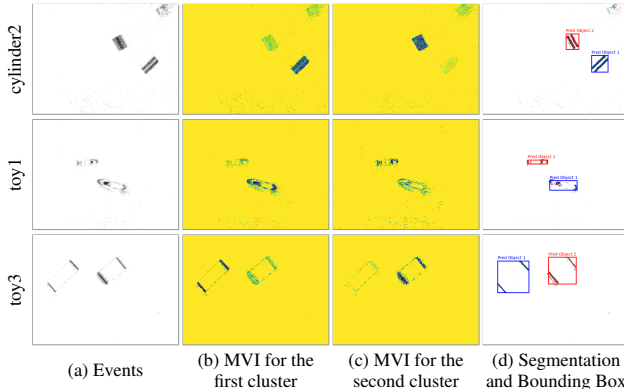


Figure 3. *Iterative clustering on self-recorded data.* (b)-(c): the mean variation images (MVIs) during two iterations show that the variation (7) becomes high (i.e., blue) for the remaining IMO (color bar in Fig. 2). We use these heat map values to produce the segmentation results (d).

small when the events are aligned with the motion parameter (b, c). The agreement between the obtained segmentation results and the bounding boxes of the moving objects demonstrates the capabilities of our method to accurately classify IMOs (d).

The comparison with previous works on motion segmentation is shown in Fig. 4 and Tab. 2. The EMSMC method [40] is highly dependent on the initial motion parameters for each cluster, resulting in unstable outcomes across different sequences. In the experiments, we test two types of initialization strategies of the motion parameters: zero initialization and random initialization, while our method is tested with zero initialization. We also compare with EMSGC.

We find that the initialization at zero is challenging for EMSMC [40]. However, regardless of the initialization strategy, the proposed method consistently provides favorable FWL scores and segmentation results, showcasing the effectiveness of the iterative segmentation approach.

4.4. Moving Object Detection

Figure 5 shows moving object detection results on the EVIMO2 dataset [5]. Here, we assume that the calibration parameters are known. Using external inputs (IMU

Method	IoU(↑)	FWL(↑)
Mitrokhin [20]	0.61	–
EMSGC [47]	0.63	–
Zhao [45]	0.62	–
Zhou [46]	0.64	–
EMSMC [40]	0.16	1.63
Ours	0.84	2.25

Table 3. *Quantitative results of moving-object detection on EVIMO2 datasets.* The proposed method produces the highest IoU among the methods compared.

and GT depth), we estimate the motion of the background events and compute the MVI of the scene, which generates clear object masks for the IMOs. Following the well-known motion field equation [43], the motion of the static background can be estimated using the scene depth $Z(\mathbf{x})$ and the camera motion (linear velocity \mathbf{V} and angular velocity $\boldsymbol{\omega}$), $\mathbf{v}(\mathbf{x}) = \frac{1}{Z(\mathbf{x})}A(\mathbf{x})\mathbf{V} + B(\mathbf{x})\boldsymbol{\omega}$. Alternatively, one can estimate the depth and camera motion via CMax (e.g., [38]), which we leave for future work. Since the background events are aligned through motion estimation, the IMOs have lower first variation, which we use to make object masks. The experimental results demonstrate that our method produces accurate segmentation and bounding box results in the three scenes. While the benchmark method struggles with segmentation in complex scenes with a large number of events, the proposed method exhibits significantly better detection of moving objects within the scenes.

Figure 6 and Tab. 3 show the comparison of moving-object detection versus prior works. The IoU is calculated using the average value across scenes containing moving objects. The proposed method achieves state-of-the-art (high) IoU values, improving by over 30%. This is also confirmed by the FWL values.

4.5. Result on the Real-world Datasets

Figure 7 provides further motion segmentation results on real-world sequences, from EMSGC [47] and ECD [23]. The EMSGC plots (first row) show the classification of the events into three clusters: background induced by the translational motion of the camera, and two pedestrians mov-

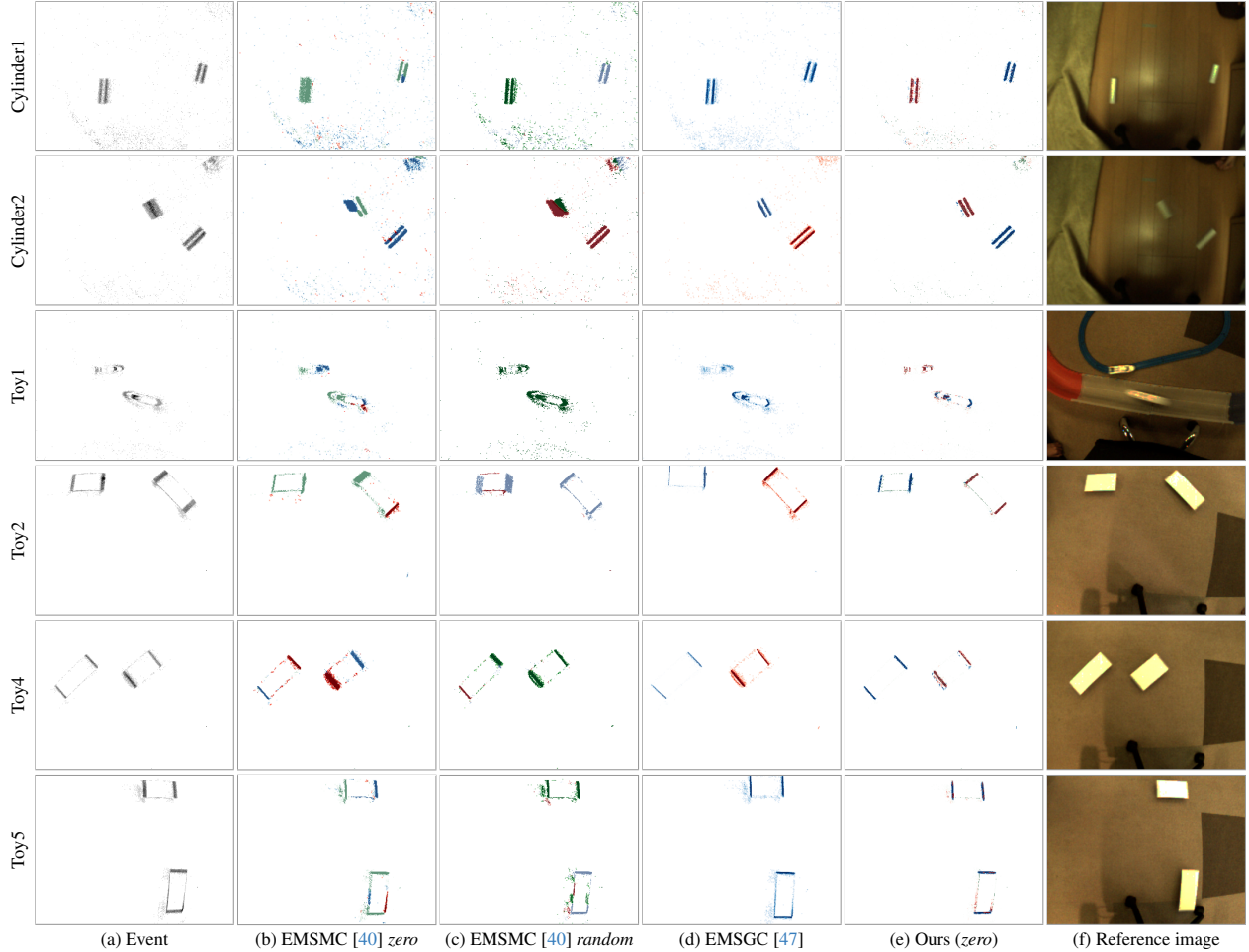


Figure 4. Segmentation results on our dataset. For benchmark, we compare with [47] and [40] using different initialization strategies.

ing in opposite directions (along with their corresponding bounding boxes). The ECD plots (second row) show the classification of the events into two clusters: the rotational motion of the camera and the dynamic motion of a person standing up. The results demonstrate that each object is successfully detected, showcasing that our method performs well on real-world data, thus indicating the potential for various applications.

However, segmentation accuracy deteriorates due to the presence of a considerable amount of event noise, resulting in small bounding boxes for IMOs in the examples. We do not fine-tune the hyperparameters of the algorithm to improve the results for these specific scenes and leave additional robustness against noise for future work.

5. Limitations

One of the primary limitations of the proposed method is its processing time. The method segments multiple mo-

tion clusters through an iterative process, leading to an increase in processing time proportional to the number of iterations (i.e., the number of distinct motions). Since the original CMax has a complexity of $O(N_e + N_p)$, the proposed method does not run in real-time. The processing times of different methods for the cylinder example (3 clusters, 4k events) on a standard CPU are: 10.27 s with the proposed method (python), 4.15 s with EMSMC (python), and 1.88 s with EMSGC (C++).

Also, classifying motions whose direction is similar is challenging. If the scene has two similar motions, the MVI (6) becomes similar among these events. Consequently, it becomes challenging to accurately classify their motions. For example, in Fig. 4 (Toy 5), two objects exhibit similar motions, making it difficult to segment them. In principle, this is a matter of the task definition (they cannot be separated just by motion, and additional cues, such as pixel distance, need to be used to segment them).

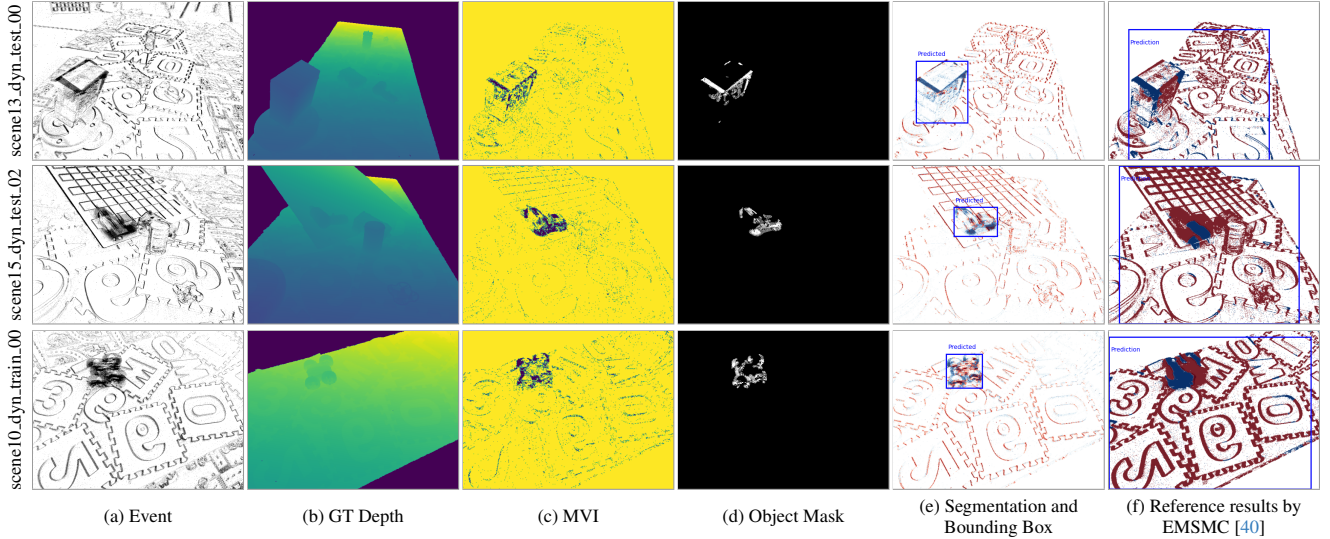


Figure 5. *Motion segmentation and moving-object detection results on the EVIMO2 dataset.* Instead of estimating the motion parameter θ , first we use the GT depth and IMU to obtain the warp for the static parts of the scene. As the MVI (c) clearly shows, the “residual” agree with the IMOs. Our segmentation results successfully detect the IMOs (e), compared with the baseline method [40].

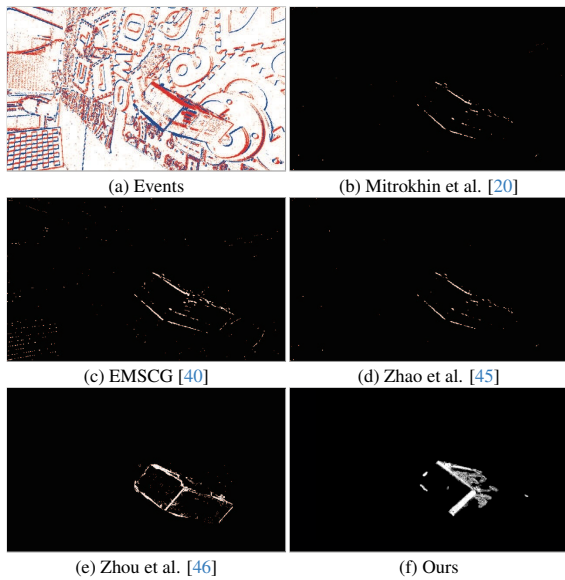


Figure 6. *Comparison with prior work on the EVIMO2 dataset.* Non-black pixels in each method are IMO. The figure is generated mimicking that in [46].

6. Conclusion

In this paper, we proposed a novel iterative motion segmentation method, based on the calculus of variations extending the Contrast Maximization framework. By classifying events into a given motion hypothesis and its residuals, the proposed method enables motion segmentation and

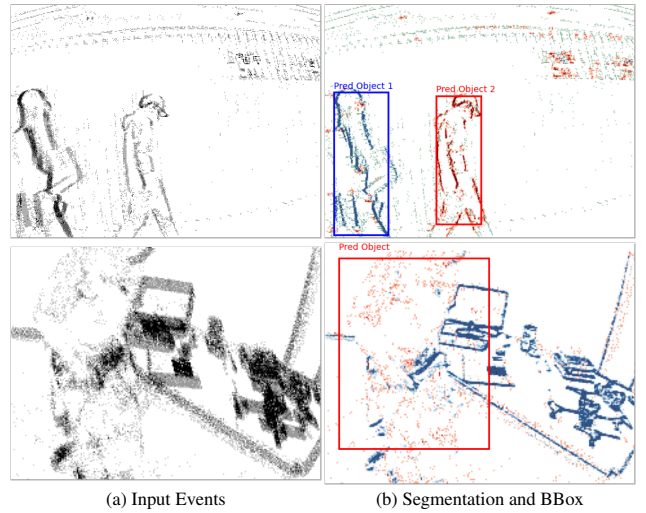


Figure 7. *Results on two real-world datasets using EMSGC [47] and ECD [23].* Due to noise, the bounding boxes become small.

moving-object detection without relying on initialization. Experimental results show that the proposed method successfully classifies event clusters both for simple datasets and publicly available datasets, producing sharp, motion-compensated images of warped events. Also, it achieves state-of-the-art accuracy for moving object detection benchmarks, with an improvement of over 30%. We hope this work broadens the capability of the CMax framework for motion segmentation, thus contributing to the theoretical advancements in event-based motion estimation.

Acknowledgments

This research was funded by the Deutsche Forschungsgemeinschaft (DFG, German Research Foundation) under Germany’s Excellence Strategy – EXC 2002/1 “Science of Intelligence” – project number 390523135.

7. Supplementary

7.1. Video

We encourage readers to watch the accompanying video, which explains the method more intuitively than the still images in the paper.

7.2. Analysis of Variations

Figure 8 shows an example histogram of variation magnitudes per event, using the box scene from EVIMO2 (*scene13_dyn_test_00* in Fig. 5). The order of raw variations is 10^{-5} , while we scale them to $[0, 255]$ for visualization as an MVI.

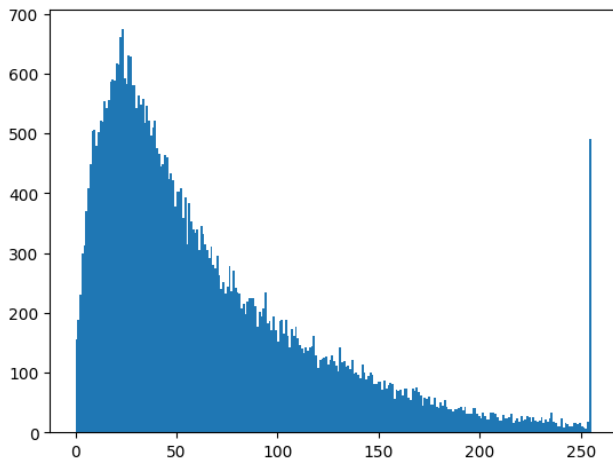


Figure 8. Histogram of the magnitude of variations per event in one sequence example from EVIMO2. The magnitude is scaled to $[0, 255]$ for visualization as an image (i.e., MVI).

8. Sensitivity Analysis

In the datasets collected from real-world environments (Secs. 4.4 and 4.5), significantly more noise is present compared to ideal conditions. The noise yields remnants of first variations being introduced during the separation of estimated motion, and hence, blurs the boundaries of motion segmentation. To address this, one may apply a simple de-noising filter using a Gaussian kernel on the IWE and classify using a certain threshold.

We evaluate the effect of the Gaussian intensity σ and the threshold of the filter on the bounding box accuracy in Fig. 9, using the EVIMO2 dataset. The experimental results show that the IoU consistently remains above 0.7 for the tested parameters (see also Sec. 4.4). We confirm that the proposed method consistently achieves the detection accuracy, even with inversely adjusting σ and the threshold.



Figure 9. Sensitivity study on the effect of threshold and sigma.

References

- [1] Yusra Alkendi, Rana Azzam, Sajid Javed, Lakmal Seneviratne, and Yahya Zweiri. Neuromorphic vision-based motion segmentation with graph transformer neural network. 2024.
- [2] Yusra Alkendi, Rana Azzam, Sajid Javed, Lakmal Seneviratne, and Yahya Zweiri. Neuromorphic vision-based motion segmentation with graph transformer neural network. *IEEE Trans. Multimedia*, 27:385–400, 2025.
- [3] Sami Arja, Alexandre Marcireau, Saeed Afshar, Bharath Ramesh, and Gregory Cohen. Motion segmentation for neuromorphic aerial surveillance. *arXiv e-prints*, 2024.
- [4] Christian Brandli, Raphael Berner, Minhao Yang, Shih-Chii Liu, and Tobi Delbruck. A 240x180 130dB 3 μ s latency global shutter spatiotemporal vision sensor. *IEEE J. Solid-State Circuits*, 49(10):2333–2341, 2014.
- [5] Levi Burner, Anton Mitrokhin, Cornelia Fermüller, and Yiannis Aloimonos. EVIMO2: An event camera dataset for motion segmentation, optical flow, structure from motion, and visual inertial odometry in indoor scenes with monocular or stereo algorithms. *arXiv e-prints*, 2022.
- [6] Lev D Elsgolc. *Calculus of Variations*. Dover Publications, Mineola, NY, 2007.
- [7] Guillermo Gallego and Davide Scaramuzza. Accurate angular velocity estimation with an event camera. *IEEE Robot. Autom. Lett.*, 2(2):632–639, 2017.
- [8] Guillermo Gallego, Henri Rebecq, and Davide Scaramuzza. A unifying contrast maximization framework for event cameras, with applications to motion, depth, and optical flow estimation. In *IEEE Conf. Comput. Vis. Pattern Recog. (CVPR)*, pages 3867–3876, 2018.
- [9] Guillermo Gallego, Mathias Gehrig, and Davide Scaramuzza. Focus is all you need: Loss functions for event-based vision. In *IEEE Conf. Comput. Vis. Pattern Recog. (CVPR)*, pages 12272–12281, 2019.
- [10] Guillermo Gallego, Tobi Delbruck, Garrick Orchard, Chiara Bartolozzi, Brian Taba, Andrea Censi, Stefan Leutenegger, Andrew Davison, Jörg Conradt, Kostas Daniilidis, and Davide Scaramuzza. Event-based vision: A survey. *IEEE Trans. Pattern Anal. Mach. Intell.*, 44(1):154–180, 2022.
- [11] Stamatiou Georgoulis, Weining Ren, Alfredo Bochicchio, Daniel Eckert, Yuanyou Li, and Abel Gawel. Out of the room: Generalizing event-based dynamic motion segmentation for complex scenes. In *Int. Conf. 3D Vision (3DV)*, pages 442–452, 2024.
- [12] Cheng Gu, Erik Learned-Miller, Daniel Sheldon, Guillermo Gallego, and Pia Bideau. The spatio-temporal Poisson point process: A simple model for the alignment of event camera data. In *Int. Conf. Comput. Vis. (ICCV)*, pages 13495–13504, 2021.
- [13] Shuang Guo and Guillermo Gallego. CMax-SLAM: Event-based rotational-motion bundle adjustment and SLAM system using contrast maximization. *IEEE Trans. Robot.*, pages 1–20, 2024.
- [14] Shuang Guo, Friedhelm Hamann, and Guillermo Gallego. Unsupervised joint learning of optical flow and intensity with event cameras. *arXiv e-prints*, 2025.
- [15] Friedhelm Hamann, Ziyun Wang, Ioannis Asmanis, Kenneth Chaney, Guillermo Gallego, and Kostas Daniilidis. Motion-prior contrast maximization for dense continuous-time motion estimation. In *Eur. Conf. Comput. Vis. (ECCV)*, pages 18–37, 2024.
- [16] Chenao Jiang, Julien Moreau, and Franck Davoine. Event-based semantic-aided motion segmentation. In *Int. Conf. Comput. Vis. Theory Appl. (VISAPP)*, 2024.
- [17] Haram Kim and H. Jin Kim. Real-time rotational motion estimation with contrast maximization over globally aligned events. *IEEE Robot. Autom. Lett.*, 6(3):6016–6023, 2021.
- [18] Diederik P. Kingma and Jimmy L. Ba. Adam: A method for stochastic optimization. *Int. Conf. Learn. Representations (ICLR)*, 2015.
- [19] Patrick Lichtsteiner, Christoph Posch, and Tobi Delbruck. A 128x128 120 dB 15 μ s latency asynchronous temporal contrast vision sensor. *IEEE J. Solid-State Circuits*, 43(2):566–576, 2008.
- [20] Anton Mitrokhin, Cornelia Fermüller, Chethan Parameshwara, and Yiannis Aloimonos. Event-based moving object detection and tracking. In *IEEE/RSJ Int. Conf. Intell. Robot. Syst. (IROS)*, pages 1–9, 2018.
- [21] Anton Mitrokhin, Chengxi Ye, Cornelia Fermüller, Yiannis Aloimonos, and Tobi Delbruck. EV-IMO: Motion segmentation dataset and learning pipeline for event cameras. In *IEEE/RSJ Int. Conf. Intell. Robot. Syst. (IROS)*, pages 6105–6112, 2019.
- [22] Anton Mitrokhin, Zhiyuan Hua, Cornelia Fermüller, and Yiannis Aloimonos. Learning visual motion segmentation using event surfaces. In *IEEE Conf. Comput. Vis. Pattern Recog. (CVPR)*, pages 14402–14411, 2020.
- [23] Elias Mueggler, Henri Rebecq, Guillermo Gallego, Tobi Delbruck, and Davide Scaramuzza. The event-camera dataset and simulator: Event-based data for pose estimation, visual odometry, and SLAM. *Int. J. Robot. Research*, 36(2):142–149, 2017.
- [24] Elias Mueggler, Guillermo Gallego, Henri Rebecq, and Davide Scaramuzza. Continuous-time visual-inertial odometry for event cameras. *IEEE Trans. Robot.*, 34(6):1425–1440, 2018.
- [25] Matthew Ng, Zi Min Er, Gim Song Soh, and Shaohui Foong. Aggregation functions for simultaneous attitude and image estimation with event cameras at high angular rates. *IEEE Robot. Autom. Lett.*, pages 1–1, 2022.
- [26] Urbano Miguel Nunes and Yiannis Demiris. Robust event-based vision model estimation by dispersion minimisation. *IEEE Trans. Pattern Anal. Mach. Intell.*, 2021.
- [27] Nobuyuki Otsu. A threshold selection method from gray-level histograms. *IEEE Trans. Systems, Man and Cybernetics*, 11(285-296):23–27, 1975.
- [28] Chethan M. Parameshwara, Simin Li, Cornelia Fermüller, Nitin J. Sanket, Matthew S. Evanusa, and Yiannis Aloimonos. SpikeMS: Deep spiking neural network for motion segmentation. In *IEEE/RSJ Int. Conf. Intell. Robot. Syst. (IROS)*, pages 3414–3420, 2021.
- [29] Chethan M. Parameshwara, Nitin J. Sanket, Chahat Deep Singh, Cornelia Fermüller, and Yiannis Aloimonos. 0-

- MMS: Zero-shot multi-motion segmentation with a monocular event camera. In *IEEE Int. Conf. Robot. Autom. (ICRA)*, pages 9594–9600, 2021.
- [30] Federico Paredes-Vallés, Jesse Hagenars, Julien Dupeyron, Stein Stroobants, Yingfu Xu, and Guido C. H. E. de Croon. Fully neuromorphic vision and control for autonomous drone flight. *Science Robotics*, 9(90):eadi0591, 2024.
- [31] Federico Paredes-Vallés, Kirk YW Scheper, Christophe De Wagter, and Guido CHE de Croon. Taming contrast maximization for learning sequential, low-latency, event-based optical flow. In *Int. Conf. Comput. Vis. (ICCV)*, pages 9661–9671, 2023.
- [32] Xin Peng, Ling Gao, Yifu Wang, and Laurent Kneip. Globally-optimal contrast maximisation for event cameras. *IEEE Trans. Pattern Anal. Mach. Intell.*, 44(7):3479–3495, 2022.
- [33] Christoph Posch, Teresa Serrano-Gotarredona, Bernabe Linares-Barranco, and Tobi Delbruck. Retinomorphing event-based vision sensors: Bioinspired cameras with spiking output. *Proc. IEEE*, 102(10):1470–1484, 2014.
- [34] Antoni Rosinol Vidal, Henri Rebecq, Timo Horstschaefer, and Davide Scaramuzza. Ultimate SLAM? combining events, images, and IMU for robust visual SLAM in HDR and high speed scenarios. *IEEE Robot. Autom. Lett.*, 3(2):994–1001, 2018.
- [35] Shintaro Shiba, Yoshimitsu Aoki, and Guillermo Gallego. A fast geometric regularizer to mitigate event collapse in the contrast maximization framework. *Adv. Intell. Syst.*, page 2200251, 2022.
- [36] Shintaro Shiba, Yoshimitsu Aoki, and Guillermo Gallego. Secrets of event-based optical flow. In *Eur. Conf. Comput. Vis. (ECCV)*, pages 628–645, 2022.
- [37] Shintaro Shiba, Yoshimitsu Aoki, and Guillermo Gallego. Event collapse in contrast maximization frameworks. *Sensors*, 22(14):1–20, 2022.
- [38] Shintaro Shiba, Yannick Klose, Yoshimitsu Aoki, and Guillermo Gallego. Secrets of event-based optical flow, depth, and ego-motion by contrast maximization. *IEEE Trans. Pattern Anal. Mach. Intell.*, 46(12):7742–7759, 2024.
- [39] Timo Stoffregen and Lindsay Kleeman. Event cameras, contrast maximization and reward functions: an analysis. In *IEEE Conf. Comput. Vis. Pattern Recog. (CVPR)*, pages 12292–12300, 2019.
- [40] Timo Stoffregen, Guillermo Gallego, Tom Drummond, Lindsay Kleeman, and Davide Scaramuzza. Event-based motion segmentation by motion compensation. In *Int. Conf. Comput. Vis. (ICCV)*, pages 7243–7252, 2019.
- [41] Timo Stoffregen, Cedric Scheerlinck, Davide Scaramuzza, Tom Drummond, Nick Barnes, Lindsay Kleeman, and Robert Mahony. Reducing the sim-to-real gap for event cameras. In *Eur. Conf. Comput. Vis. (ECCV)*, pages 534–549, 2020.
- [42] Gemma Taverni, Diederik Paul Moeys, Chenghan Li, Celso Cavaco, Vasyl Motsnyi, David San Segundo Bello, and Tobi Delbruck. Front and back illuminated Dynamic and Active Pixel Vision Sensors comparison. *IEEE Trans. Circuits Syst. II*, 65(5):677–681, 2018.
- [43] Emanuele Trucco and Alessandro Verri. *Introductory Techniques for 3-D Computer Vision*. Prentice Hall PTR, Upper Saddle River, NJ, USA, 1998.
- [44] Ziyun Wang, Jinyuan Guo, and Kostas Daniilidis. UnEVIMO: Unsupervised event-based independent motion segmentation. In *Eur. Conf. Comput. Vis. (ECCV)*, 2024.
- [45] Chunhui Zhao, Yakun Li, and Yang Lyu. Event-based real-time moving object detection based on imu ego-motion compensation. In *IEEE Int. Conf. Robot. Autom. (ICRA)*, pages 690–696, 2023.
- [46] Hanyu Zhou, Zhiwei Shi, Hao Dong, Shihan Peng, Yi Chang, and Luxin Yan. JSTR: Joint spatio-temporal reasoning for event-based moving object detection. In *IEEE Int. Conf. Robot. Autom. (ICRA)*, pages 10650–10656, 2024.
- [47] Yi Zhou, Guillermo Gallego, Xiuyuan Lu, Siqi Liu, and Shaojie Shen. Event-based motion segmentation with spatio-temporal graph cuts. *IEEE Trans. Neural Netw. Learn. Syst.*, pages 1–13, 2021.
- [48] Alex Zihao Zhu, Nikolay Atanasov, and Kostas Daniilidis. Event-based visual inertial odometry. In *IEEE Conf. Comput. Vis. Pattern Recog. (CVPR)*, pages 5816–5824, 2017.